

Estimating the open magnetic flux from the interplanetary and ionospheric conditions

C. Wang,¹ Z. Y. Xia,^{1,2} Z. Peng,¹ and Q. M. Lu²

Received 13 February 2013; revised 23 March 2013; accepted 29 March 2013.

[1] The open magnetic flux (F_{PC}) is a key parameter to study magnetospheric dynamical process, which is closely related to magnetic reconnections in the dayside magnetopause and magnetotail. Using global MHD simulations, we find that the open magnetic flux F_{PC} can be estimated through a combined parameter f by $F_{PC} = 0.89f/(f + 0.20) + 0.52$, where the parameter $f = v_{SW} B_S n_{SW}^{1/5} \Sigma_P^{1/3}$ is a function of the solar wind velocity (v_{SW}), the solar wind number density (n_{SW}), the southern interplanetary magnetic field (IMF) strength (B_S), and the ionospheric Pederson conductance (Σ_P). The comparison with the limited observational F_{PC} data available in the literature shows its promise in estimating the open magnetic flux from the interplanetary and ionospheric conditions. The open magnetic flux (F_{PC}) may be served as a key space weather forecast element in the future.

Citation: Wang, C., Z. Y. Xia, Z. Peng, and Q. M. Lu (2013), Estimating the open magnetic flux from the interplanetary and ionospheric conditions, *J. Geophys. Res. Space Physics*, 118, doi:10.1002/jgra.50255.

1. Introduction

[2] The open magnetic flux connecting the interplanetary space with the geospace is one of the important parameters that characterize the state of magnetosphere. The open magnetic flux is formed mainly by the reconnection occurring at the dayside magnetopause between the interplanetary magnetic field (IMF) and the Earth's magnetic field. When there is a large angle shear between the IMF and the Earth's field lines, especially when the IMF is southward, the dayside reconnection changes field topology, making terrestrial field lines from closed to open, which connects directly with the interplanetary field lines. The open field lines are stretched into the magnetotail by the solar wind flow and reclosed by the reconnection in the neutral sheet and then return to the dayside again. This cycle of field lines' opening and closing was proposed by *Dungey* [1961, 1963] and is named the Dungey cycle. The relationship between the open magnetic flux (F_{PC}), the dayside reconnection rate (Φ_D), and the nightside reconnection rate (Φ_N) can be expressed by a statement of Faraday's law as

$$\frac{dF_{PC}(t)}{dt} = \Phi_D(t) - \Phi_N(t)$$

[*Siscoe and Huang*, 1985]. Clearly, the magnitude of the open magnetic flux increases when the rate Φ_D exceeds Φ_N and decreases the other way around. Moreover, when the reconnection rates Φ_D and Φ_N are approximately equal, the

amount of open flux does not change significantly, and the magnetosphere reaches a quasi-steady state. The rate Φ_D is mainly determined by the upstream solar wind conditions, and Φ_N is controlled by the magnetotail conditions. Φ_N is used to describe the rate of open magnetic flux annihilation, while Φ_D describes its accumulation [*Lockwood and Cowley*, 1992; *Milan et al.*, 2003, 2007, 2008; *Gordeev et al.*, 2011]. When the IMF is southward, the dayside reconnection creates more open magnetic flux, resulting in the expansion of the polar cap and the accumulation of large amount of open magnetic flux in the magnetotail. Generally, this tail loading is followed by transient explosive unloading with high reconnection rate, which removes the overmuch open magnetic flux. When the rates of dayside and nightside reconnection are nearly equal, and the reconnections at the two sides thus balance each other, a quasi-steady state with almost a constant amount of open magnetic flux in the magnetosphere will then be reached. Certainly, the magnitude of the open magnetic flux in the quasi-steady state is associated with the solar wind conditions to a large extent.

[3] *DeJong et al.* [2007] studied the open magnetic flux in three types of events, namely, isolated substorms, sawtooth, and SMC (steady magnetospheric convection) events, and found that in the individual sawtooth, which has a stronger solar wind driving, the amount of open magnetic flux is larger than those in the other two types of events. *Huang et al.* [2009] also analyzed the open magnetic flux in the three types of events and did a data fitting between the amount of open magnetic flux and the merging electric field which is regarded as the controller of the dayside reconnection rate. The merging electric field is defined as $E_m = V_{SW} (B_y^2 + B_z^2)^{1/2} \sin^2(\theta_c/2)$ [*Kan and Lee*, 1979], where V_{SW} is the solar wind velocity, B_y and B_z are the IMF components, and θ_c is the IMF clock angle. The fitting shows a positive correlation between the open magnetic flux and the merging electric field, as would be expected. Furthermore, a

¹State Key Laboratory of Space Weather, Center for Space Science and Applied Research, Chinese Academy of Sciences, Beijing, China.

²School of Earth and Space Sciences, University of Science and Technology of China, Hefei, China.

Corresponding author: C. Wang, State Key Laboratory of Space Weather, Center for Space Science and Applied Research, Chinese Academy of Sciences, Beijing 100190, China. (cw@spaceweather.ac.cn)

superposed epoch analysis by *Milan et al.* [2009] indicated that the open magnetic flux governs the substorm intensity, and its level is controlled by the solar wind conditions. A larger solar wind velocity and density and more negative IMF Bz can increase the open magnetic flux and cause more intense substorms. Although the magnetosphere is not in a steady state during the time periods of substorms and sawtooth events, the overall levels of the open magnetic flux in these events have a good relevance with the solar wind conditions as well.

[4] In addition to the above-mentioned discussions on the open magnetic flux observationally, global MHD simulations are effective tools to distinguish the open-close field line boundary (OCB) and further calculate the area of polar cap and the amount of the open magnetic flux. *Rae et al.* [2004, 2010] compared OCB defined by observations and model calculations in several steady events and found a good agreement between them. *Kabin et al.* [2004] studied the relationship between the OCB and the solar wind parameters using the BATS-R-US MHD model [*Powell et al.*, 1999] and showed that a southward IMF Bz and increasing solar wind dynamic pressure could lead to a growth of polar cap area. *Merkin and Goodrich* [2007] used the LFM global MHD model to analyze the relationship between the polar cap area (A_{pc}) and the strength of interplanetary electric field (IEF) in steady conditions and found a saturation phenomenon of the polar cap area as the IEF strength increases. They also did a simple analysis of effects of the solar wind dynamic pressure and ionospheric conductance. The previous work deepen our understanding of the open magnetic flux and their relationship with the solar wind and ionospheric conditions; however, the overall quantitative relationship has not been established yet.

[5] In this paper, we use the PPMLR-MHD model to simulate the solar wind-magnetosphere-ionosphere (SMI) system and study 180 cases which are quasi-steady states with due southward IMF. We then try to establish an empirical formula from simulation results to estimate the amount of the open magnetic flux from the solar wind and ionospheric conditions and finally try to validate it with observational data available in the literature.

2. Methodology and Results

2.1. Simulation Model

[6] The global MHD simulation model used in this study is the PPMLR-MHD model developed by *Hu et al.* [2005, 2007]. This model employs the Lagrangian version of the piecewise parabolic method (PPMLR) developed by *Colella and Woodward* [1984] to MHD. The PPM algorithm has an accuracy of the third order in space and the second order in time, with a much lower numerical dissipation than traditional numerical schemes. The detail of this model could be found in our previous work [e.g., *Hu et al.*, 2007], but the main simplifying assumptions used in the simulations are summarized as follows: (1) The solar wind is along the Sun-Earth line, (2) the inner boundary of the computational domain is taken to be $3 R_E$ (R_E is the radius of the Earth) to avoid the complexity associated with the plasma-sphere and the constrained time step imposed by the strong magnetic field, (3) the ionosphere is uniform with Pedersen conductance only, and (4) the coupling between the inner

magnetosphere and ionosphere employs an electrostatic model, which maps the field-aligned current J_{\parallel} from the inner boundary to the ionosphere, and maps the electric potential from the ionosphere to the inner boundary along the Earth's dipole field lines. The flow velocity in the inner boundary is then set to be $\mathbf{v} = \mathbf{E} \times \mathbf{B}_d / B_d^2$ (\mathbf{B}_d is the dipole field).

[7] The computations continue for more than 5 h in physical time for each run until a quasi-steady state is reached, when the relative changes of key parameters such as the magnetic field, density, velocity, etc. are less than 5% for the time interval of about half an hour. Each solution can be described by interplanetary and ionospheric parameters, including Σ_P of the ionospheric Pedersen conductance, the solar wind density n_{sw} , velocity v_{sw} , and the south component of IMF B_S . We conducted a total of 180 numerical runs, with different combinations of Σ_P (1, 5, and 10 S), n_{sw} (5, 10, 15, and 20 cm^{-3}), v_{sw} (400, 600, and 800 km s^{-1}), and B_S (5, 10, 15, 20, and 25 nT). The computation domain is set to be $-300 R_E < x < 30 R_E$, $-150 R_E < y, z < 150 R_E$ in the GSE coordinates. It is divided into $160 \times 162 \times 162$ grid points: a uniform mesh is used in the near Earth domain within $10 R_E$, with a constant spacing of $\delta = 0.4 R_E$, and the grid spacing outside increases as a geometrical series with a common ratio 1.05 along each axis.

[8] In order to define the open magnetic flux from the simulation results, we trace all the magnetic field lines from the foot points at the inner boundary by using the Runge-Kutta method. The foot points are set to be $r = 3.1 R_E$; the longitude varies from 0° to 360° and the latitude from 90° to 0° , with an interval of 1° between two adjacent points in one hemisphere. The outer boundary is set to be $-40 R_E < x < 20 R_E$, $-30 R_E < y, z < 30 R_E$ in an attempt to reduce the amount of calculations. If a field line finally returns to the inner boundary in the opposite hemisphere, it is then regarded as a closed magnetic field line; otherwise, it is categorized as an open magnetic field line. We sum up $\mathbf{B} \cdot d\mathbf{s}$ (\mathbf{B} , $d\mathbf{s}$ are the magnetic field and the normal area vector, respectively) of all the open flux units and thus obtain the total amount of the open magnetic flux (F_{PC}).

[9] In the process of estimating the F_{PC} from the simulation results, we must set an outer boundary subjectively. The outer boundary must be not too large to improve the efficiency of our calculations; on the other hand, the outer boundary must be large enough to ensure that the field lines that flow out of the boundary are open ones. To examine the effects of the outer boundary, we have randomly selected 10 cases and calculated the F_{PC} with larger outer boundaries. The results show that the values of F_{PC} do not vary in a significant way in all these cases. We are thus confident that the outer boundary chosen in this study is large enough, and the estimation of F_{PC} is reasonably accurate.

2.2. Empirical Formula From Simulation Results

[10] More than 20 candidate solar wind-magnetosphere coupling functions and their correlation coefficients to some state variables including the polar cap (PC) size have been proposed during the last decades [*Newell et al.*, 2007]. In the work of *Newell et al.* [2007], a function $v^{4/3} B_T^{2/3} \sin^{8/3}(\theta_c/2)$, which is named $d\Phi_{MP}/dt$, is the best fitting of the PC size with a correlation coefficient of 0.614. We therefore believe that any new formula must include the $v_{sw}^\alpha B_S^\beta$ element,

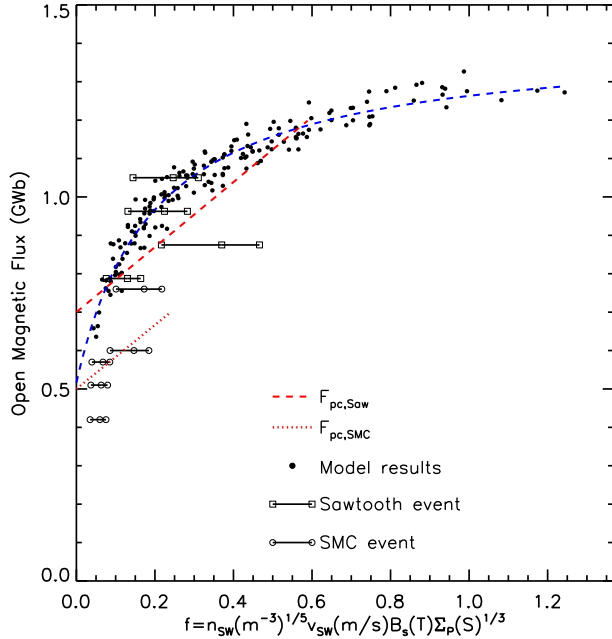


Figure 1. Relationship between F_{PC} and the combined parameter f . The black dots denote the simulation data, the square and circle symbol lines represent the observational data of the sawtooth and SMC events, respectively. The three points of line stand for different Σ_p parameters, which are 1, 5, and 10 S from left to right. The blue curve indicates the empirical formula between F_{PC} and f . The red dashed and dotted lines are plotted according to the work of *Huang et al.* [2009]; see text for details.

where α and β are two constant indices to be determined by trial and error method. Due to the positive correlation of F_{PC} to v_{SW} and B_S , the index α and β must be positive. By comparing outcomes of different sets of values of α and β , we find that the appropriate values of α and β are both equal to 1. It turns out that the final form $v_{SW}B_S$ is just the solar wind electric field E_{SW} .

[11] As demonstrated in our simulation results, we find that the solar wind number density n_{SW} and the ionospheric conductance Σ_p have moderate effects on F_{PC} , which is consistent with the finding of *Merkin and Goodrich* [2007]. In order to improve the prediction accuracy, we multiply $n_{SW}^\gamma \Sigma_p^\delta$ with E_{SW} and find that the appropriate values for γ and δ are 1/5 and 1/3, respectively. Therefore, we finally obtain a combined parameter f , which is defined as $f = v_{SW}B_S n_{SW}^{1/5} \Sigma_p^{1/3}$. The F_{PC} distribution of our simulation data as a function of f is shown in Figure 1, presented by the black dots. Unlike scattered patterns when plotting against other parameters, the black dots tend to be centralized to form a clear curve.

[12] When the combined parameter f is small, the F_{PC} increases linearly with the combined parameter f . After f reaches a threshold value, the growth rate begins to decrease, and F_{PC} remains a nearly constant value in the end, which is regarded as the saturation of F_{PC} . Therefore, we conclude the form of the function between F_{PC} and f to be

$$F_{PC} = \frac{Af}{f+B} + C$$

[13] After testing various values of A , B , and C , we find that the best combination of A , B , and C is that $A = 0.89$, $B = 0.20$, and $C = 0.52$. The blue dashed curve in Figure 1 represents this function, which is a good fitting of the black dots with the correlation coefficient of 0.97. According to this expression, when f is much smaller than $B = 0.2$, F_{PC} grows with f at a rate of about $A/B \approx 4.5$; when f increases near to and over B , the rate decreases, and the F_{PC} finally saturates at a value of about $A + C \approx 1.4$ GWb. The root mean square (RMS) deviation of the data points from the fitting curve is about 0.04 GWb, and the relative RMS deviation is about 3.3%. The deviation may be caused by various reasons. First, it is impossible that the SMI system can reach a truly steady state in simulations; it instead fluctuates with time [*Hu et al.*, 2005], and therefore the F_{PC} also oscillates with time. This kind of deviation can be decreased by calculating an average value of F_{PC} of several different time steps, as what was done by *Merkin and Goodrich* [2007]. Other important sources of the deviation may come from the method to calculate F_{PC} and the simpleness of our empirical function including both the form of f and the relationship between f and F_{PC} .

[14] To assess the intensity of the oscillation in our model, we analyze the last six time steps data of 21 randomly selected events and calculate the coefficient of variance C.V. (the ratio of the standard deviation to the mean) of F_{PC} . Most of the cases (17 of 21) have a C.V. smaller than 3%, and the average C.V. of all these 21 cases is about 2.4%. We therefore believe that our simulated results are qualified to be used to study the F_{PC} variation of different quasi-steady states.

2.3. Comparison With Observations

[15] In order to test the validation of the empirical formula inferred from the simulation results, we try to compare our simulated data of F_{PC} to the observational data available in the published literature (to our knowledge). *Huang et al.* [2009] has analyzed the amount of open magnetic flux of three sorts of events, the sawtooth, isolated substorms, and steady magnetospheric convection (SMC) events. The SMC and sawtooth events are both driven by a long period of time of continuously southward and reasonably steady IMF [*Henderson*, 2004; *Henderson et al.*, 2006]. In SMC events, the amount of F_{PC} remains almost constant, but in sawtooth events, the amount of F_{PC} fluctuates around an average level. Since our simulations are for quasi-steady states only, we select the data of SMC and sawtooth events (though not as steady as SMC events, the entire level of the parameters can keep nearly constant during the events' periods) for comparison. The SMC events may occur in a weak magnetic driving condition with the merging electric field in the range 0–6 mV/m, and the sawtooth events may occur when the magnetic driving is much more intense and the range of merging electric field is 2–14 mV/m. The work of *Huang et al.* [2009] gave the relationship between open magnetic flux (values at onsets for sawtooth events and average values for SMC events) and merging electric field and offered a fitting of it. The fitting functions are $F_{PC,SMC} = 0.50 + 3.27 \times 10^{-2} E_m$ for SMC events and $F_{PC,Saw} = 0.80 + 4.07 \times 10^{-2} E_m$ for sawtooth events. For sawtooth events, the total open magnetic flux is reduced by 24–26% after the expansion onset, so to characterize the average open magnetic flux level, we multiply 87.5% to the $F_{PC,Saw}$ value to estimate the average

Table 1. List of Events and Their Observational Data Which Are Used to Compare With the Simulation Results

Data	Starting Time	Type	B_s (nT)	v_{sw} (km/s)	n_{sw} (cm^{-3})	F_{PC} (GWb)	Reference
3 Feb 1998	16:30	SMC	5.91	319.88	2.83	0.51	<i>DeJong et al. [2008]</i>
15 Feb 1998	00:00	SMC	3.80	371.71	9.28	0.42	<i>DeJong et al. [2008]</i>
17 Feb 1998	15:45	SMC	8.24	394.68	12.27	0.60	<i>DeJong et al. [2008]</i>
26 Oct 2000	03:00	SMC	5	400	3	0.57	<i>DeJong et al. [2007, 2009]</i>
22 Dec 2000	21:42	SMC	11.58	318.25	15.42	0.76	<i>DeJong et al. [2008]</i>
18 Apr 2001	00:00	sawtooth	15	500	20	1.0	<i>Hubert et al. [2008]</i>
22 Oct 2001	11:06	sawtooth	10	600	5	1.1	<i>DeJong et al. [2007]</i>
19 Apr 2002	12:05	sawtooth	10	600	8	1.15	<i>DeJong et al. [2009]</i>
24 Oct 2002	11:20	sawtooth	5	650	7	0.9	<i>Hubert et al. [2008]</i>

F_{PC} value of a sawtooth event. The above two expressions are also plotted in Figure 1, in red dashed and dotted lines, respectively, taking the average solar wind number density for both events and $\Sigma_p = 5$ S. In addition, we also find some specific examples including five SMC and four sawtooth events to test our estimation formula. These events are obtained from *Hubert et al. [2008]* and *DeJong et al. [2007, 2008, 2009]* and are listed in Table 1. The values of F_{PC} , n_{sw} , v_{sw} , and B_s are all obtained from these papers; some of them are provided directly, and some of them are estimated by reading approximately from the figures in the papers. However, we could not confirm the Σ_p values in practice, because the Σ_p varies both spatially and temporally, so we try all the values of Σ_p in our simulations, which are 1 S, 5 S, and 10 S. These observational data are added to Figure 1. The square symbol lines are for sawtooth data, and the circle symbol lines are for SMC events. The plotted observational open magnetic flux values are 87.5% of the maximums for sawtooth events and the average value for SMC data. For each event, there are three f values corresponding to the three Σ_p values, and from left to right are 1 S, 5 S, and 10 S in sequence. Generally speaking, the simulated data are larger than SMC events data and fit much better to the sawtooth events data. This is likely due to weaker effects of Σ_p and n_{sw} on F_{PC} than that of E_{sw} . However, the number of the events is not enough to draw a certain conclusion, and more observational data are needed to make plausible explanations.

3. Summary

[16] We investigate the open magnetic flux (F_{PC}) as functions of interplanetary and ionospheric conditions based on the PPMLR-MHD simulations. We calculate the values of F_{PC} for 180 quasi-steady states of the SMI system with different parameters—the solar wind velocity (v_{sw}), the solar wind number density (n_{sw}), the south IMF strength (B_s), and the ionospheric Pederson conductance (Σ_p).

[17] In order to estimate the magnitude of the open magnetic flux F_{PC} , we coin up a combined parameter $f = v_{sw} B_s n_{sw}^{1/5} \Sigma_p^{1/3}$, which is a function of the interplanetary and ionospheric conditions. The open magnetic flux F_{PC} can then be expressed as $F_{PC} = 0.89f/(f + 0.20) + 0.52$. As expected, the open flux F_{PC} is controlled mainly by the solar wind electric field $E_{sw} = v_{sw} B_s$, which is close related to the dayside reconnection rate. As f becomes larger, the growth rate of F_{PC} decreases, and finally, F_{PC} saturates at a value of about 1.4 GWb.

[18] To further test the validation of the empirical formula inferred from the simulation results, we compare our simulated data of F_{PC} to some observational data available in the published literature. The results agree well with the observations of sawtooth events but not very well for SMC events. The simulation runs in this study are limited to simplest cases; many complex settings are ignored. For example, we do not allow for the complicated IMF and solar wind conditions, the effect of Hall conductance, and the nonuniformity of the ionospheric conductance. Nevertheless, we have given a reasonable approximation of the open magnetic flux based on the interplanetary and ionospheric conditions, which may be served as a key space weather forecast element in the future.

[19] **Acknowledgments.** This work was supported by 973 program 2012CB825602, NNSFC grant 41231067 and 41004073, and in part by the Specialized Research Fund for State Key Laboratories of China. Masaki Fujimoto thanks the reviewers for their assistance in evaluating this paper.

References

- Colella, P., and P. R. Woodward (1984), The piecewise parabolic method (PPM) for gas-dynamical simulations, *J. Comput. Phys.*, *54*, 174–201.
- DeJong, A. D., X. Cai, R. C. Clauer, and J. F. Spann (2007), Aurora and open magnetic flux during isolated substorms, sawtooth, and SMC events, *Ann. Geophys.*, *25*, 1865–1876.
- DeJong, A. D., A. J. Ridley, and C. R. Clauer (2008), Balanced reconnection intervals: Four case studies, *Ann. Geophys.*, *26*, 3897–3912.
- DeJong, A. D., A. J. Ridley, X. Cai, and C. R. Clauer (2009), A statistical study of BRIs (SMCs), isolated substorms, and individual sawtooth injections, *J. Geophys. Res.*, *114*, A08215, doi:10.1029/2008JA013870.
- Dungey, J. W. (1961), Interplanetary magnetic fields and the auroral zones, *Phys. Rev. Lett.*, *6*, 47–48.
- Dungey, J. W. (1963), The structure of the exosphere or adventures in velocity space, in *Geophysics, The Earths Environment*, edited by C. De Witt, J. Hieblot, and L. Le Beau, 503 p., Gordon and Breach, New York.
- Gordeev, E. I., V. A. Sergeev, T. I. Pulkkinen, and M. Palmroth (2011), Contribution of magnetotail reconnection to the cross-polar cap electric potential drop, *J. Geophys. Res.*, *116*, A08219, doi:10.1029/2011JA016609.
- Henderson, M. G. (2004), The May 2–3, 1986 CDAW-9C interval: A sawtooth event, *Geophys. Res. Lett.*, *31*, L11804, doi:10.1029/2004GL019941.
- Henderson, M. G., G. D. Reeves, R. Skoug, M. T. Thomsen, M. H. Denton, S. B. Mende, T. J. Immel, P. C. Brandt, and H. J. Singer (2006), Magnetospheric and auroral activity during the 18 April 2002 sawtooth event, *J. Geophys. Res.*, *111*, A01S90, doi:10.1029/2005JA011111.
- Hu, Y. Q., et al. (2005), Oscillation of quasi-steady Earths magnetosphere, *Chin. Phys. Lett.*, *22*(10), 2723–2726.
- Hu, Y. Q., X. C. Guo, and C. Wang (2007), On the ionospheric and reconnection potentials of the Earth: Results from global MHD simulations, *J. Geophys. Res.*, *112*, A07215, doi:10.1029/2006JA012145.
- Huang, C.-S., A. D. DeJong, and X. Cai (2009), Magnetic flux in the magnetotail and polar cap during sawtooth, isolated substorms, and steady magnetospheric convection events, *J. Geophys. Res.*, *114*, A07202, doi:10.1029/2009JA014232.

- Hubert, B., S. E. Milan, A. Grocott, S. W. H. Cowley, and J. C. Gérard (2008), Open magnetic flux and magnetic flux closure during sawtooth events, *Geophys. Res. Lett.*, *35*, L23301, doi:10.1029/2008GL036374.
- Kabin, K., R. Rankin, G. Rostoker, R. Marchand, I. J. Rae, A. J. Ridley, T. I. Gombosi, C. R. Clauer, and D. L. DeZeeuw (2004), Open-closed field line boundary position: A parametric study using an MHD model, *J. Geophys. Res.*, *109*, A05222, doi:10.1029/2003JA010168.
- Kan, J. R., and L. C. Lee (1979), Energy coupling function and solar wind-magnetosphere dynamo, *Geophys. Res. Lett.*, *6*(7), 577–580, doi:10.1029/GL006i007p00577.
- Lockwood, M., and S. W. H. Cowley (1992), Ionospheric convection and the substorm cycle, in *Proceedings of the International Conference on Substorms (ICS- 1)*, pp. 99–109, EAS Spec. Publ., SP- 335, Kiruna, Sweden.
- Merkin, V. G., and C. C. Goodrich (2007), Does the polar cap area saturate? *Geophys. Res. Lett.*, *34*, L09107, doi:10.1029/2007GL029357.
- Milan, S. E., M. Lester, S. W. H. Cowley, K. Oksavik, M. Brittnacher, R. A. Greenwald, G. Sofko, and J.-P. Villain (2003), Variations in polar cap area during two substorm cycles, *Ann. Geophys.*, *21*, 1121–1140, doi:10.5194/angeo-21-1121-2003.
- Milan, S. E., G. Provan, and B. Hubert (2007), Magnetic flux transport in the Dungey cycle: A survey of dayside and nightside reconnection rates, *J. Geophys. Res.*, *112*, A01209, doi:10.1029/2006JA011642.
- Milan, S. E., P. D. Boakes, and B. Hubert (2008), Response of the expanding/contracting polar cap to weak and strong solar wind driving: Implications for substorm onset, *J. Geophys. Res.*, *113*, A09215, doi:10.1029/2008JA013340.
- Milan, S. E., A. Grocott, C. Forsyth, S. M. Imber, P. D. Boakes, and B. Hubert (2009), A superposed epoch analysis of auroral evolution during substorm growth, onset and recovery: Open magnetic flux control of substorm intensity, *Ann. Geophys.*, *27*, 659–668.
- Newell, P. T., T. Sotirelis, K. Liou, C.-I. Meng, and F. J. Rich (2007), A nearly universal solar wind-magnetosphere coupling function inferred from 10 magnetospheric state variables, *J. Geophys. Res.*, *112*, A01206, doi:10.1029/2006JA012015.
- Powell, K. G., P. L. Roe, T. J. Linde, T. I. Gombosi, and D. L. DeZeeuw (1999), A solution-adaptive upwind scheme for ideal magnetohydrodynamics, *J. Comput. Phys.*, *154*, 284–309.
- Rae, I. J., K. Kabin, R. Rankin, F. R. Fenrich, W. Liu, J. A. Wanliss, A. J. Ridley, T. I. Gombosi, and Z. De D. L. (2004), Comparison of photometer and global MHD determination of the open-closed field line boundary, *J. Geophys. Res.*, *109*, A01204, doi:10.1029/2003JA009968.
- Rae, I. J., et al. (2010), Comparison of the open-closed separatrix in a global magnetospheric simulation with observations: The role of the ring current, *J. Geophys. Res.*, *115*, A08216, doi:10.1029/2009JA015068.
- Siscoe, G. L., and T. S. Huang (1985), Polar cap inflation and deflation, *J. Geophys. Res.*, *90*, 543–547.